
Universiteit
Leiden
The Netherlands

G 292.0 + 1.8 - Evidence for a pseudo-Crab stage in SNR evolution

Braun, R.; Goss, W.M.; Caswell, J.L.; Roger, R.S.

Citation
Braun, R., Goss, W. M., Caswell, J. L., & Roger, R. S. (1986). G 292.0 + 1.8 - Evidence for a pseudo-Crab stage in SNR evolution. *Astronomy And Astrophysics*, *162*, 259-264. Retrieved from https://hdl.handle.net/1887/6840

Version:	Not Applicable (or Unknown)
License:	Leiden University Non-exclusive license
Downloaded from:	https://hdl.handle.net/1887/6840

Note: To cite this publication please use the final published version (if applicable).

1986A&A...162..259B

Astron. Astrophys. 162, 259–264 (1986)

ASTRONOMY AND ASTROPHYSICS

G 292.0+1.8: evidence for a pseudo-Crab stage in SNR evolution

R. Braun[1,*], **W.M. Goss**[2], **J.L. Caswell**[3], **and R.S. Roger**[4]

[1] Sterrewacht Leiden, Postbus 9513, 2300 RA Leiden, The Netherlands
[2] Kapteyn Astronomical Institute, Postbus 800, 9700 AV Groningen, The Netherlands
[3] Division of Radiophysics, CSIRO, PO Box 76, Epping, NSW 2121, Australia
[4] Dominion Radio Astrophysical Observatory, Penticton, BC, V2A 6K3, Canada

Received January 2, accepted February 15, 1986

Summary. New observations of the young type II supernova remnant (SNR) G292.0+1.8 have been made at 843 MHz with 0'.8 resolution using the Molonglo Observatory Synthesis Telescope (MOST) and at 12, 25, 60, and 100 μm with IRAS. All of the available structural and kinematic data suggests that the southwest portion of the SNR is encountering the periphery of a cloud (where $n = 0.4\,\mathrm{cm}^{-3}$) while the northeast portion is expanding into low density intercloud gas ($n < 0.003\,\mathrm{cm}^{-3}$). A relatively small mass ($< 1\,M_{\odot}$) of high velocity ejecta seems responsible for the blast wave. A significant mass of slower ejecta is now encountering the reverse shock in the southwest, giving rise to a center-filled morphology. Such a pseudo-Crab phase may be a common occurrence in type II SNR of intermediate age.

Key words: supernova remnants – G292.0+1.8 – dust

1. Introduction

Early radio surveys (Milne, 1969; Shaver and Goss, 1970) led to the discovery of the southern galactic supernova remnant G292.0 +1.8. Subsequent radio observations (Lockhart et al., 1977) revealed a peculiar, apparently center-filled morphology which led to the suggestion that the SNR may be Crab-like (although the radio spectral index, $\alpha = 0.37$, is rather steep for objects of this class). Optical observations (Goss et al., 1979; Murdin and Clark, 1979; Van den Bergh, 1979; Braun et al., 1983) have revealed a system of high velocity oxygen rich knots reminiscent of those found in Cas A (Chevalier and Kirshner, 1978), suggesting a relatively young SNR and a massive progenitor. Observations of strong emission lines in the thermal X-ray spectrum (Clark et al., 1980) also suggest a massive progenitor, while ruling out the Crab-like classification. The X-ray image (Touhy et al., 1982) indicates an over-all morphology which is similar to that seen in the radio; bright central knots and an extended plateau.

While a large body of observational data exists for the SNR, the origin of the various emission processes has not yet been satisfactorily accounted for. In this paper we present new radio and infrared observations which we analyze in the context of all available observational constraints and in the framework of numerical simulations of pre-adiabatic SNR evolution. The observations and data reduction techniques are described in Sect. 2. In Sect. 3 we begin by considering the distance, environment and geometry of G292.0+1.8 and then go on to discuss the brightness distribution in the various wavelength bands and the physical parameters we derive. Our conclusions are summarized in Sect. 4.

Send offprint requests to: R. Braun

* Now at National Radio Astronomy Observatory, PO Box O, Socorro, NM 87801, USA

2. Observations and data reduction

2.1. Radio data

The radio observations were carried out using the Molonglo Observatory Synthesis Telescope (MOST, Durdin et al., 1984) of the University of Sydney on 27 August, 1984. The flux density calibration was carried out using the point source 1934–63 with an assumed flux density of 13.55 Jy at 843 MHz. After an observation of 12 h with a field of view of 46′ × 54′ ($\alpha \times \delta$) the rms noise is 1.3 mJy and the synthesized beam 43″ × 50″ ($\alpha \times \delta$). The measured dynamic range is somewhat better than 100:1. The map was processed by "CLEAN" ing the field using an observation of 1934–63 extending over 12 hours as the point source response. The resulting map is shown in Fig. 1.

2.2. Infrared data

A one degree square field centered on G292.0+1.8 was extracted from the IRAS Skyflux maps (HCON3, IRAS, 1985) in the 12, 25, 60, and 100 μm bands for further processing. The gridded point source response is similar in the four bands, with FWHM ~ 6′. Straightforward analysis of the data is hampered by a number of sources of confusion. Besides star images which affect localized areas at 12 and 25 μm, the ubiquitous zodiacal light emission introduces a varying background across the field and worse still, cool dust emission with structure on all observable scale sizes is present in most directions. The problem of background confusion was addressed by using the four maps to carry out a spectral decomposition by least squares into three component maps, on the basis of their distinct spectral character (as discussed by Braun, 1986). The three components which were so extracted were; 1) cool dust, peaking longward of 100 μm, 2) zodiacal light, peaking between 12 and 25 μm and 3) the shock-heated dust emission of the SNR, peaking between 25 and 60 μm. Initial

© European Southern Observatory • Provided by the NASA Astrophysics Data System

1986A&A...162..259B

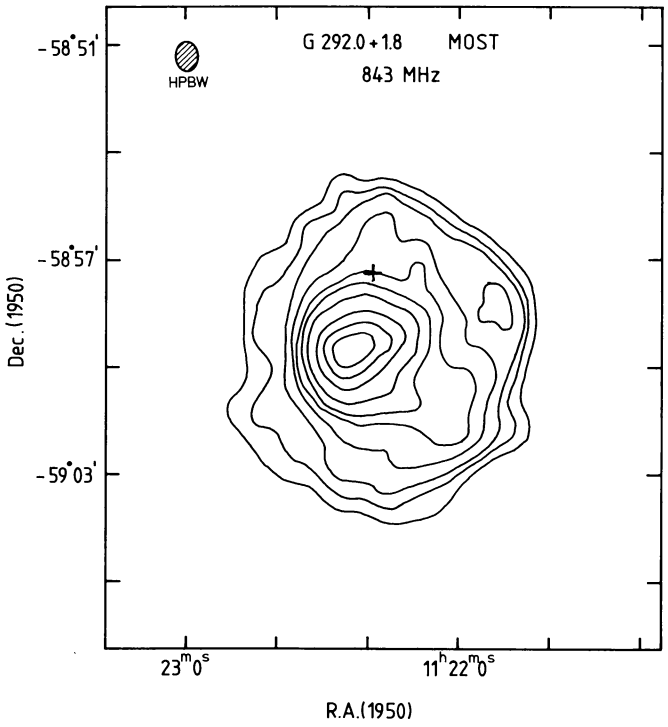

Fig. 1. Radio brightness distribution. The 843 MHz MOST map (HPBW $= 43'' \times 50''$) with contours at 20, 40, 60, 100, 150, 200, 300, 500, 700, and 900 mJy/beam. Note the central ridge and extended plateau. The nominal expansion center is indicated by the cross

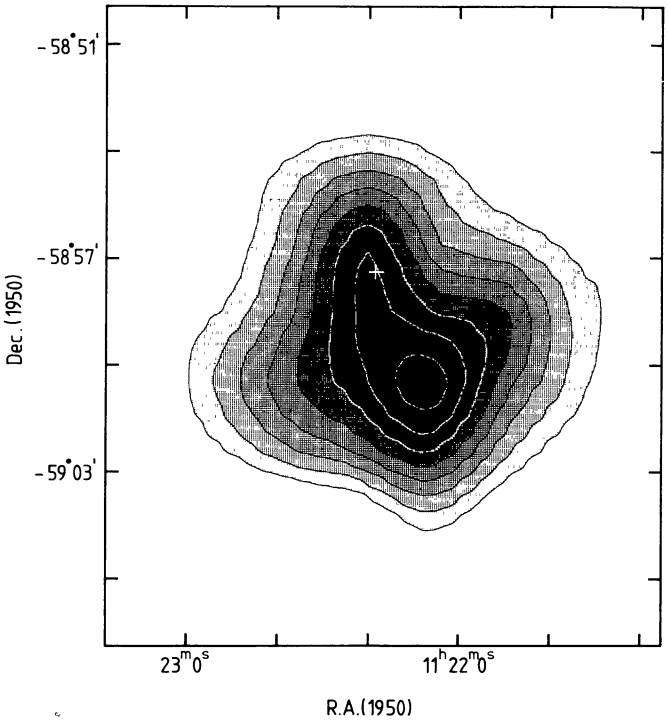

Fig. 3. Distribution of shock-heated dust. The background corrected (see Sect. 2.2) 60 μm IRAS image (HPBW ~ 6'). Contours are in units of nominal surface brightness. The linear contour levels and grey scale transitions are at 2.25 to 7.5 MJy/sr in steps of 0.75 MJy/sr. Note the overall coincidence with the radio plateau but displacement of peak to the south-west. The nominal expansion center is indicated by the cross

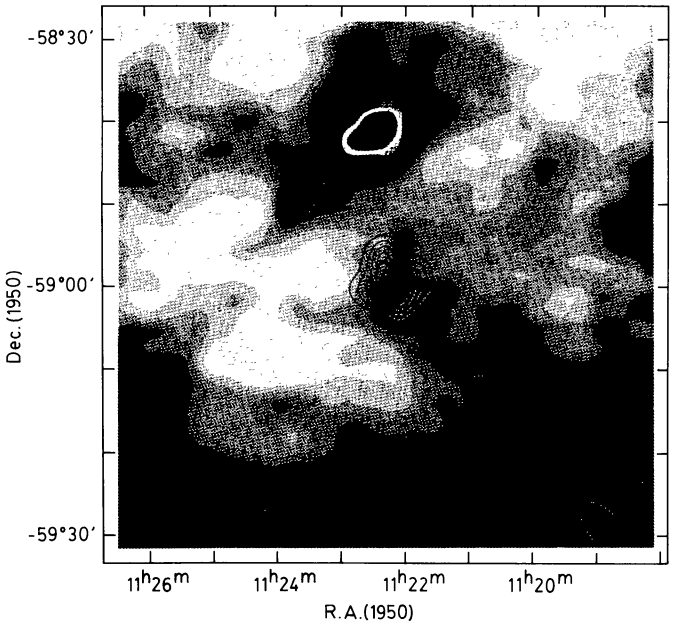

Fig. 2. G292.0+1.8 and its environment. The grey scale represents cool dust emission, (with transitions occurring at 49, 59, 61, 63, 65, 68, and 74 MJy/sr at 100 μm) while the contours represent a warmer component (with linear contour levels at 3 to 10 MJy/sr in steps of 1 MJy/sr at 60 μm) as derived from the spectral decomposition (see Sect. 2.2) of IRAS data at 12, 25, 60, and 100 μm. A cool arm of dust (and gas) extends up from the galactic plane to the SNR at center. No attempt was made to model the emission of the H II region to the north. The nominal expansion center is indicated by the cross

Table 1. Infrared spectral parameters

Nominal flux density [Jy]	(12 μm)	<0.42
	(25 μm)	15.1
	(60 μm)	38.2
	(100 μm)	14.0
Color corrected flux [Jy]	(12 μm)	<0.32
	(25 μm)	18.0
	(60 μm)	35.0
	(100 μm)	12.6
Color corrected λI_λ [W m^{-2} sr^{-1}]	(12 μm)	$<5.47\ 10^{-8}$
	(25 μm)	$1.48\ 10^{-6}$
	(60 μm)	$1.20\ 10^{-6}$
	(100 μm)	$2.59\ 10^{-7}$
λ_{peak} [μm]		36 ± 1
λI_λ^{max} [W m^{-2} sr^{-1}]		$2.16\ 10^{-6}$
Angular radius [arcmin]		5.5

estimates of the component spectra were iteratively adjusted so as to obtain featureless residuals and strictly positive component maps with a minimum degree of correlation with each other. Map areas containing bright stars or H II regions were not represented by the three component spectra and could therefore not be fit simultaneously. Such (isolated) map areas will not be considered in the subsequent analysis. The cool and shock-heated components so derived are overlaid in Fig. 2. The four input maps were

© European Southern Observatory • Provided by the NASA Astrophysics Data System

1986A&A...162..259B

background corrected by subtracting scaled versions of the cool dust component and a quadratic surface fit to the zodiacal light component from each. Accurate integrated flux densities could then be derived against a nearly featureless background in all four IRAS bands. The 60 μm band background corrected map is shown in Fig. 3.

The nominal integrated fluxes were color-corrected by comparison with inband integrations of a model spectrum. The model was generated from an MRN (Mathis et al., 1977) size distribution of silicate and graphite grains at a fixed temperature using the absorption efficiencies derived by Draine and Lee (1984) and tabulated by Draine (1985). The same model was used to derive the wavelength where the spectrum peaks, $\lambda_{\rm peak}$ and the peak surface brightness, $\lambda I_\lambda^{\rm max}$ (see Braun, 1986 for a more complete discussion). The nominal and color-corrected fluxes are listed in Table 1 together with the parameters of the spectral peak.

3. Discussion

3.1. Distance, environment, and geometry

The available constraints on the distance to G292.0+1.8 are the H I absorption properties (Caswell et al., 1975) and the optical absorption inferred from [O II] and [O III] emission line strengths (Goss et al., 1979; Murdin and Clark, 1979). The neutral hydrogen absorption seen against the radio continuum emission consists of the local contribution at $V_{\rm lsr} = 0\,{\rm km\,s^{-1}}$ and a narrow peak centered at $V_{\rm lsr} = -30\,{\rm km\,s^{-1}}$. The fractional absorption in the line, together with the line width and brightness temperature seen in emission imply an H I column density $N_{\rm H} \simeq 8\ 10^{20}\,{\rm cm^{-2}}$ for this feature. However, the Schmidt (1965) rotation curve predicts a most negative velocity of $V_{\rm lsr} = -20\,{\rm km\,s^{-1}}$ at a distance, $D = 3.7\,{\rm kpc}$ along this line of sight. The departures from simple rotation, in accordance with the above model, are therefore $\geqq 10\,{\rm km\,s^{-1}}$. As the minimal estimate of departure is almost certainly over-optimistic, the range of acceptable lower limits to the distance are those which lie within about $15\,{\rm km\,s^{-1}}$ of the narrow absorption feature, i.e. $D_{\rm min} \geqq 3.7 \pm 2\,{\rm kpc}$. The narrowness and non-multiplicity of the profile suggest that the lower part of this range in distance is perhaps most appropriate.

The derivation of optical absorption on the basis of the forbidden oxygen line ratios in collisionally ionized gas is difficult. Current modelling of the intrinsic line ratios (eg. Raymond, 1979; Shull and McKee, 1979) has illustrated the dependence of line intensities on a wide variety of parameters, while comparison of SNR spectra with these models has illustrated remaining inadequacies, especially in regard to the [O II] and [O III] lines (e.g. Dennefeld, 1982). Simple considerations have however been employed to derive a very approximate visual absorption, $A_V = 2 \pm 2\,{\rm mag}$ (Murdin and Clark, 1979). In conjunction with a mean interstellar absorption in this direction of 0.5 mag/kpc (Goss et al., 1979 and references therein) a distance, $D = 4 \pm 4\,{\rm kpc}$ is inferred.

The environment of the SNR is well illustrated by the distribution of cool dust (Fig. 2) derived from the spectral decomposition of the IRAS images in the 12, 25, 60, and 100 μm bands. The galactic plane emission is seen in the south and a probably unrelated H II region complex in the north. An arm of emission extends up from the galactic plane to the position of the SNR. The shock-heated dust of the SNR (also in Fig. 2) is seen immediately to the northeast of and partially overlapping the brightest emission from this arm. Since previous studies have shown that moderate to high ISM densities ($n > 0.2\,{\rm cm^{-3}}$) are required for observable emission from shock-heated dust (Braun, 1986) this morphological coincidence is quite suggestive of a physical association. The excess surface brightness of the galactic arm at 100 μm, $I = 10\,{\rm MJy\,sr^{-1}}$ with respect to the diffuse background, corresponds to an H I column density, $N_{\rm H} \simeq 10^{21}\,{\rm cm^{-2}}$ (and $A_V = 0.5\,{\rm mag}$) assuming an approximately local ISRF (interstellar radiation field, cf. Draine and Anderson, 1985). Since this is the only distinct feature visible at the position of the SNR, and the estimated column density is in good agreement with that seen in H I absorption, it seems likely that this is the same cloud and that it lies immediately in front of and below the remnant. Since 0.5 mag of extinction is then occurring in the immediate vicinity of the SNR, the estimated visual absorption (above) implies the somewhat lower distance, $D = 3 \pm 4\,{\rm kpc}$, while the H I value is no longer simply a lower limit.

Considering both of the above constraints suggests the distance, $D = 3.6 \pm 1.5\,{\rm kpc}$. At this distance, the 12′ dimensions of the galactic arm correspond to $13 \pm 5\,{\rm pc}$. Assuming a similar depth along the line-of sight implies a cloud density, $n_{\rm H} = 20 \pm 8\,{\rm cm^{-3}}$. The cloud ends abruptly at the position of the SNR, suggesting that densities must be significantly lower to the northeast.

3.2. Brightness distribution

The peculiar brightness distribution of G292.0+1.8 at all observed wavelengths has not allowed a simple morphological classification of the SNR type.

The Einstein HRI image (Tuohy et al., 1982) consists of a system of bright knots and arcs superposed on a faint elliptical plateau with no clear indication for limb-brightening at the periphery. The analysis of X-ray data for other young SNR has indicated that the bright clumps which are often observed are most likely associated with knots of ejecta encountering the interface between diffuse ejecta and the shocked ISM (e.g. Seward et al., 1983), while the outer shock itself is either not seen at all or only faintly under favorable circumstances. The Einstein SSS spectrum (Clark et al., 1980) of G292.0+1.8 supports the view that the bulk of its X-ray emission is due to an enriched, thermal plasma, ie. shocked ejecta from the inner layers of a massive progenitor.

The optical morphology is well illustrated by the [O II] λ3727 image of Murdin and Malin (private communication) shown in Fig. 4. The brightest emission is concentrated in "streamers" extending to the south and east of the bright X-ray knots. Just as in some of the fast moving knots (FMK) in Cas A, the optical spectrum of this material consists almost exclusively of the forbidden lines of O and Ne (Goss et al., 1979; Murdin and Clark., 1979). The spectrum and high radial velocities of this material (Murdin and Clark, 1979; Braun et al., 1983) together imply that it represents knots of high density ejecta undergoing recombination after being shocked on encountering a diffuse high density zone, presumably the inner surface of the diffuse ejecta/shocked ISM layer. The abrupt "turn-on" of the "streamers" to the south and east of the X-ray knots suggests that the optical knots are propagating in these directions and that the arc defined by their northwest edge delineates the inner surface of the high density zone. Braun et al. (1983) have shown that a dominant component of systematic expansion is apparent in the radial velocity data if an expansion center lying to the northwest of this interface is assumed at $\alpha_{50} = 11^{\rm h}22^{\rm m}18 \pm 2^{\rm s}$, $\delta_{50} = -58°57'25 \pm 15''$. This position is marked in Figs. 1–3.

The radio morphology is well illustrated in the 843 MHz map shown in Figs. 1 and 4. A bright central ridge is elongated along the ridge of [O II] and X-ray emission, while a faint plateau extends

© European Southern Observatory • Provided by the NASA Astrophysics Data System

1986A&A...162..259B

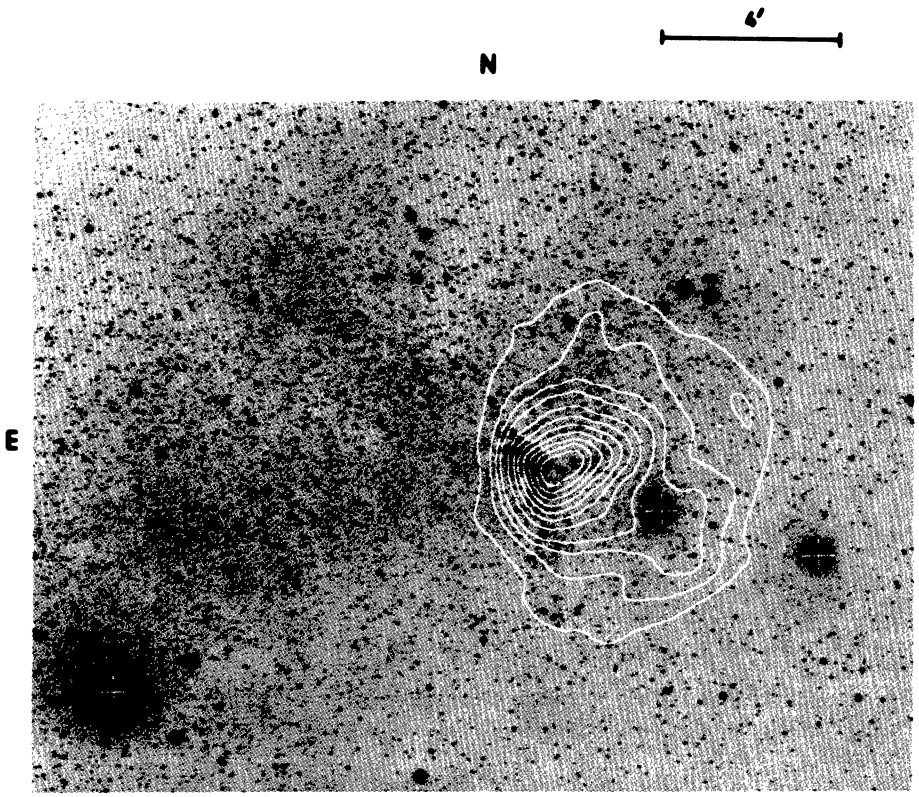

Fig. 4. Radio and optical morphology. Contours of the 843 MHz MOST map (at 5, 10, 15, 20, 30, 40, ... 90 % of the peak brightness of 1.08 Jy/beam) overlaid on the [O II] λ3727 interference filter photograph (courtesy of Murdin and Malin) obtained at the prime foxus of the AAT. "Streamers" of recombining knots extend to the south and east of the bright central concentration

over roughly 10′, coincident with that seen in the X-ray image. A total flux density at 843 MHz of $S_{843} = 15.5 \pm 0.6$ Jy was found; in good agreement with the spectrum presented by Lockhart et al. (1977) ($\alpha = -0.37$, $S \propto \nu^{\alpha}$) which predicts $S_{843} = 15.9$ Jy. This is divided between the bright ridge of (deconvolved) angular size $2\farcm0 \times 1\farcm6$ (centered at $\alpha_{50} = 11^{h}22^{m}22^{s}9 \pm 3^{s}$, $\delta_{50} = -58°59'31'' \pm 2''$ with p.a. $= 120°$) with a flux density $S^{C}_{843} = 6.2 \pm 0.5$ Jy, and the plateau (approx. 10 arcmin diameter) with flux density $S^{P}_{843} = 9$ Jy. A search for spectral index variations between 843 and 1415 MHz was carried out with a smoothed version of the map in Fig. 3 and the Fleurs λ21 cm map (Lockhart et al., 1977). Over this restricted frequency range there is no evidence for significant variations in spectral index within ± 0.2. The spectrum of both the central and plateau components is therefore almost certainly nonthermal. In addition, Shaver (private communication) has searched for the H109α recombination line using the Parkes 64 m telescope at 6 cm with a 4 arcmin beam. No line was detected with an upper limit of 0.03 K (T_B). If a hypothetical thermal source had an electron temperature and velocity width typical of galactic H II regions, then a line to continuum ratio of ~ 0.05 would be expected. The upper limit is, however, an order of magnitude less than this value. Thus, since the plateau contributes about 50 % of the peak intensity as observed with a 4′ beam, it appears that less than 20–30 % of the emission could arise from a conventional H II region.

Similar to the case of X-ray emission, the radio emission from other young SNR is dominated by bright clumps associated with the interaction between ejecta and the inner surface of the diffuse shell. The region between this interface and the outer shock may be filled with diffuse emission, while the outer shock itself can only rarely be distinguished (cf. Braun, 1986).

The distribution of shock-heated dust is illustrated by the background corrected 60 μm image shown in Fig. 3. A diffuse plateau is seen which is approximately coextensive with the X-ray/radio plateau. The peak of the distribution is, however, located at $\alpha_{50} = 11^{h}22^{m}09^{s}+1^{s}$, $\delta_{50} = -59°00'25'' \pm 10''$ to the southwest of the brightest radio and X-ray emission. The recurring pattern found in other young SNR (Braun, 1986) is that the brightest dust emission is associated with the layer of shocked ISM between the inner ejecta surface and the outer shock.

All of the available evidence suggests that the bright "central" region of G292.0+1.8 is actually the current active interface where the inward propagating reverse shock is encountering relatively slowly (~ 2000 km s^{-1}) expanding clumpy ejecta. The outer shock is roughly delineated in the southwest by the extent of the diffuse radio, X-ray and shock-heated dust emission, while to the northeast, the ambient densities are so low that negligible deceleration and thus emission has occurred. The expansion center of the system must lie to the north of the arc seen in optical, radio and most clearly in the X-ray emission. We will adopt the center of curvature of this arc at $\alpha_{50} = 11^{h}22^{m}18^{s} \pm 2^{s}$, $\delta_{50} = -58°57'25''$ $\pm 15''$ as the nominal expansion center.

3.3. *Physical parameters*

The relative radii of the inner ejecta surface and outer shocks in the southern portion of G292.0+1.8 indicate that a relatively large mass ratio $X = M_{ISM}/M_0$ of swept-up to ejected diffuse mass has been acquired locally. The radial velocity data for the optical knots is well fit by a spatial-velocity ellipsoid of radius $\theta = 2\farcm6$ and velocity $V = 2200$ km s^{-1} (Braun et al., 1983) with respect to the nominal expansion center above. Since the knots are now recombining, their space velocities must have been ~ 200 km s^{-1} greater before being shocked on encountering this surface. Combining an original space velocity $v^{0}_{FMK} = 2400$ km s^{-1} with the radius $r_i = 2.7 \pm 1.1$ pc (at the distance $D = 3.6 \pm 1.5$ kpc) yields an age $\tau = 1100 \pm 460$ yr. The angle averaged radial cut through the

© European Southern Observatory • Provided by the NASA Astrophysics Data System

1986A&A...162..259B

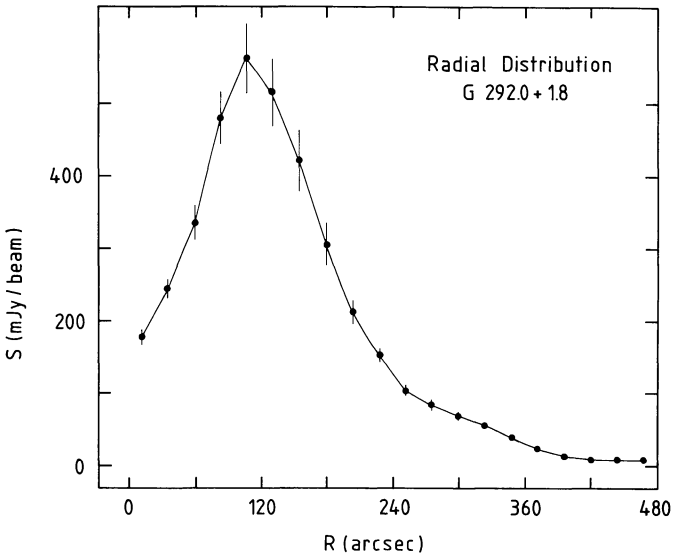

Fig. 5. Angle averaged radial profile through the 843 MHz map of Fig. 1 with respect to the nominal expansion center at $\alpha_{50} = 11^h22^m18^s$, $\delta_{50} = -58°57'25''$ (marked in Figs. 1–3) and averaged over position angles, $\phi = 100$ to 225. Note the thick inner shell consistent with radius $\theta \simeq 150''$ and the edge of the outer shelf at $\theta \simeq 330''$

radio brightness distribution shown in Fig. 5 indicates a thick shell structure with an implied radius consistent with that found for the optical knots. The faint plateau, however, is seen to extend to a radius of $\theta \simeq 5'.5$, or $r_s = 5.8 \pm 2.4$ pc.

Formulae describing the pre-adiabatic evolution of supernova remnants are given by Braun (1986) based on previously published one-dimensional numerical simulations. Two useful expressions (his equations B.7 and B.8) are those relating shock radius r_s and velocity v_s to the original shock velocity v_0 and current mass ratio X.

$$r_s = v_0 (0.75 - 0.127 \log^2 X) X^{-0.195} t, \quad (1)$$

$$v_s = 0.6\, v_0 (0.75 - 0.127 \log^2 X) X^{-0.338}. \quad (2)$$

Comparison of the current ratio of inner ejecta to shock radii, $r_i/r_s = 0.47$ with the values in Table B.1 of Braun (1986) implies a mass ratio, $X \sim 13.5$. Equation (1) can then be used to derive the original shock velocity, $v_0 = 14{,}400$ km s^{-1} which corresponds to a current shock velocity, $v_s = 2100$ km s^{-1} via Eq. (2). (It should be noted that the above quantities X, v_0 and v_s are independent of the distance.) While the original expansion velocity is somewhat higher than that found by Braun (1986) for Cas A (10,900 $\pm$ 1000 km s^{-1}), it is still within the range of velocities observed for the outer layers of SN II ejecta, 10,000 to 15,000 km s^{-1} (e.g. Searle, 1974).

The infrared spectral data for the shock-heated dust emission (listed in Table 1) corresponds to a spectral peak at $\lambda_{peak} = 36.0 \pm 1\,\mu$m with a maximum surface brightness $\lambda I_\lambda^{max} = 2.16 \pm 0.20\ 10^{-6}$ W m^{-2} sr^{-1}. Draine (1981) and Braun (1986) have discussed how these observable parameters are related to the physical parameters of interest, namely the local shock velocity, v_c pre-shock density, n_c and volume filling factor, f_c. The appropriate expressions are (Eqs. (4a), (4c), and (5) from Braun 1986),

$$\lambda I_\lambda^{max} \simeq 3.34\ 10^{-6} f_c \left(\frac{\tau}{400\,\mathrm{yr}}\right)\left(\frac{n_c}{\mathrm{cm}^{-3}}\right)^2 \left(\frac{v_c}{10^3\,\mathrm{km\,s}^{-1}}\right)^3 \mathrm{W\,m}^{-2}\,\mathrm{sr}^{-1} \quad (3a)$$

for $n_c\tau < 5\ 10^2$ cm^{-3} yr and $v_c \gtrsim 1800$ km s^{-1}

$$\lambda I_\lambda^{max} \simeq 3.48\ 10^{-5} f_c \left(\frac{n_c}{\mathrm{cm}^{-3}}\right)\left(\frac{v_c}{10^3\,\mathrm{km\,s}^{-1}}\right)^3 \mathrm{W\,m}^{-2}\,\mathrm{sr}^{-1} \quad (3b)$$

for $n_c\tau > 5\ 10^4$ cm^{-3} yr and

$$\lambda_{peak} \simeq 37.6 \left(\frac{n_c}{\mathrm{cm}^{-3}}\right)^{-0.18} \left(\frac{v_c}{10^3\,\mathrm{km\,s}^{-1}}\right)^{-0.3} \mu\mathrm{m}. \quad (4)$$

Since the shock velocity derived above is based on the southern periphery where infrared emission is brightest (cf. Fig. 3) it should be appropriate for the gas with which the dust is mixed. Equation (4) can then be used to derive the pre-shock gas density, $n_c = 0.37$ cm^{-3}. The absence of a discernible reverse shock interface in the northeast suggests that the local mass ratio must be, $X_{NE} \leqq 1$. The ratio of current shock radii can then be derived from equation 1 yielding $r_{NE}/r_{SW} \geqq 2.1$. The volume encountered by the two hemispheres will scale as this ratio cubed, so that the density must be a factor $X_{SW}(r_{NE})^3/X_{NE}(r_{SW})^3 > 130$ less, i.e. $n_{NE} < 0.003$ cm^{-3}. Such a density is consistent with current estimates of the intercloud density in a three phase ISM (e.g. McKee and Ostriker, 1977).

The volume filling factor of the dusty gas can be derived from Eq. (3a), yielding $f_c = 0.2 \pm 0.1$, a value consistent with substantial filling to the southwest. The pre-shock density found above implies a "uniform" swept-up mass $M_{ISM} = \frac{4}{3}\pi r^3 \mu m_H n_c = 10^{+17}_{-8}\, M_\odot$ (with a mean molecular weight $\mu = 1.3$) so that the mass of ejecta dynamically coupled to the ISM is $M_0 = 0.7^{+1.3}_{-0.55}\, M_\odot$ (using the mass ratio, $X = 13.5$ from above). The current kinetic energy of the swept-up ISM assuming approximately adiabatic internal density and velocity profiles is given by (cf. Braun, 1986),

$$E_K^{ISM} = 0.0450 \left(\frac{r}{2\,\mathrm{pc}}\right)^3 \left(\frac{n_c}{\mathrm{cm}^{-3}}\right)\left(\frac{v_c}{10^3\,\mathrm{km\,s}^{-1}}\right)^2 10^{50}\,\mathrm{erg} \quad (5)$$

yielding $E_k^{ISM} = 1.8^{+3.0}_{-1.4}\ 10^{50}$ erg corresponding to an original energy $E_0 = E_k^{ISM}/0.28 = 6.4^{+11}_{-5}\ 10^{50}$ erg. The cubic dependence on the uncertain distance is responsible for the large uncertainties in the quantities above. However, it is clear that a relatively small mass (in relation to the SN II progenitor mass) $M_0 < 1\,M_\odot$ was involved in powering the blast wave. This is similar to the finding of Braun (1986) for the historical SNR, Tycho, Kepler, and Cas A, all of which indicate (dynamically coupled) ejecta masses $M_0 \simeq 0.35\,M_\odot$. A similar mass estimate would be inferred for G 292.0 + 1.8 if a distance $D = 2.9$ kpc were adopted. Such a low distance seems quite plausible. On the other hand, if the far distance $D \sim 5$ kpc is adopted, an ejecta mass $M_0 = 1.8\,M_\odot$ and initial energy $E_0 = 1.7\ 10^{51}$ erg are implied. The quantities derived above are summarized in Table 2.

4. Conclusions

The available morphological and kinematic evidence suggests that G 292.0 + 1.8 is near the edge of an interstellar cloud. The southwestern portion of the SNR appears to be encountering the cloud periphery ($n_c = 0.37$ cm^{-3}) and has evolved to the point that the reverse shock, associated with the bright X-ray/radio rim, is at approximately half the outer shock radius. This is in contrast to younger galactic SNR where the reverse shock is still at $\geqq 70\,\%$ of the outer shock radius (cf. Braun, 1986). The northeastern portion is expanding into an intercloud region where the low densities ($n < 0.003$ cm^{-3}) can neither support immersed dust nor generate

© European Southern Observatory • Provided by the NASA Astrophysics Data System

1986A&A...162..259B

Table 2. Derived physical parameters

Distance [kpc]	3.6 ± 1.5	
Age [yr]	1100 ± 460	
Initial expansion velocity [km s^{-1}]	14,400	
Diffuse ejecta Mass [$M_\odot$]	$0.7^{+1.3}_{-0.55}$	
E_k^0 of diffuse Ejecta [10^{50} erg]	6.4^{+11}_{-5}	
	South-west	North-east
ISM density [cm^{-3}]	0.37	<0.003
Current shock velocity [km s^{-1}]	2100	>6500

significant emission through deceleration (except perhaps in hard X-rays). A relatively small mass of diffuse ejecta $M_0 \leqq 1\,M_\odot$ has determined the early dynamical evolution of the SNR although the current emission processes (excepting the infrared) are dominated by the slow, clumpy ejecta now encountering the reverse shock. This process has given rise to a center-filled morphology (actually a thick one-sided shell in this instance), which may be a common occurrence for the remnants of type II SN during intermediate evolutionary times (where the mass ratio $X = 10 \rightarrow 30$). Such objects are clearly not "Crab-like" as their appearance might suggest (although the slowly expanding clumpy ejecta are likely to form the basis of such objects as well) and can most easily be distinguished from their pulsar driven counterparts by their thermal X-ray spectrum.

The evaporation and/or ablation of the remaining ejecta should contribute to the internal energy of the SNR, except when it is sufficiently clumpy to penetrate the outer shock and so escape the system. This suggests a gradual increase in the internal energy available for driving the shock in pre-adiabatic SNR even in the absence of evaporation of engulfed interstellar clouds.

There are indications that the G292.0+1.8 the SN energy was abnormally high. A refined distance estimate based on a proper motion study of the fast-moving optical knots would help to resolve this question as well as more fully constrain the geometry.

Acknowledgements. We would like to thank Prof. B.Y. Mills and the late Prof. A.G. Little for help in organizing these observations. RB acknowledges the financial support of the Netherlands Foundation for Astronomical Research (ASTRON) which is supported by the Netherlands Organization for the Advancement of Pure Research (Z.W.O.). WMG acknowledges support for a visit to Australia from CSIRO, Division of Radiophysics. The Molonglo Radio Observatory is supported by the Australian Research Grants Scheme, by the University of Sydney and by the Science Foundation for Physics within the University of Sydney.

References

Braun, R., Goss, W.M., Danziger, I.J., Boksenberg, A.: 1983, in *Supernova Remnants and their X-ray Emission*, eds. J. Danziger, P. Gorenstein, Reidel, Dordrecht, p. 159
Braun, R.: 1986, *Astron. Astrophys.* (submitted)
Caswell, J.L., Murray, J.D., Roger, R.S., Cole, D.J., Cooke, D.J.: 1975, *Astron. Astrophys.* **45**, 239
Chevalier, R.A., Kirshner, R.P.: 1978, *Astrophys. J.* **234**, 493
Clark, D.H., Tuohy, I.R., Becker, R.H.: 1980, *Monthly Notices Roy. Astron. Soc.* **193**, 129
Dennefeld, M.: 1982, *Astron. Astrophys.* **112**, 215
Draine, B.T.: 1981, *Astrophys. J.* **245**, 880
Draine, B.T., Lee, H.M.: 1984, *Astrophys. J.* **285**, 89
Draine, B.T., Anderson, N.: 1985, *Astrophys. J.* **292**, 494
Draine, B.T.: 1985, *Astrophys. J. Suppl.* **57**, 587
Durdin, J.M., Little, A.G., Large, M.I.: 1984, in *Indirect Imaging*, ed. J.A. Roberts, Cambridge Univ. Press, p. 75
Goss, W.M., Shaver, P.A., Zealey, W.J. Murdin, P., Clarke, D.H.: 1979, *Monthly Notices Roy. Astron. Soc.* **188**, 357
IRAS Explanatory Supplement, 1985, eds. Beichman, C.A., Neugebauer, G., Habing, H.J., Clegg, P.E., Chester, T.J.
Lockhart, I.A., Goss, W.M., Caswell, J.L., McAdam, W.B. 1977, *Monthly Notices Roy. Astron. Soc.* **179**, 147
Mathis, J.S., Rumpl, W., Nordsieck, K.H.: 1977, *Astrophys. J.* **217**, 425
McKee, C.F., Ostriker, J.P.: 1977, *Astrophys. J.* **218**, 148
Milne, D.K.: 1969, *Australian J. Phys.* **22**, 613
Murdin, P., Clark, D.H.: *Monthly Notices Roy. Astron. Soc.* **189**, 501
Raymond, J.C.: 1979, *Astrophys. J. Suppl.* **39**, 1
Schmidt, M.: 1965, in *Galactic Structure-Stars and Stellar Systems V*, eds. A. Blaauw, M. Schmidt, Chicago, Univ. of Chicago Press
Searle, L.: 1974, in *Supernovae and Supernova Remnants*, ed. C.B. Cosmovici, Reidel, Dordrecht, p. 125
Seward, F., Gorenstein, P., Tucker, W.: 1983, *Astrophys. J.* **266**, 287
Shaver, P.A., Goss, W.M.: 1970, *Australian J. Phys. Astrophys. Suppl.* **14**, 133
Shull, J.M., McKee, C.F.: 1979, *Astrophys. J.* **227**, 131
Tuohy, I.R., Clark, D.H., Burton, W.M.: 1982, *Astrophys. J.* **260**, L65
van den Bergh, S.: 1979, *Astrophys. J.* **234**, 493

© European Southern Observatory • Provided by the NASA Astrophysics Data System